CHEMISTRY OF MATERIALS

Article

pubs.acs.org/cm

Synthesis and Stoichiometry of Different Layered Sodium Cobalt Oxides

Yuechuan Lei, Xin Li, Lei Liu, and Gerbrand Ceder*

Department of Materials Science and Engineering, Massachusetts Institute of Technology, Cambridge, Massachusetts 02139, United States

ABSTRACT: Layered Na−metal oxides can form in different crystal structures, each with different electrochemical behavior. As a prototype system to better understand how each phase can be formed, we present the conditions under which different layered phases of Na_xCoO_2 can be stabilized in solid-state synthesis. Using a novel combination of ex situ XRD on as-synthesized samples, with in situ XRD to monitor the relation between Na content and lattice parameters, we are able to construct a phase diagram of Na_xCoO_2 between 450 to 750 °C in air and for Na:Co sample ratios ranging from 0.60 to 1.05. Four single phase domains of O3, O′3, P′3, and P2 are revealed based on the XRD analysis. In contrast to previous reports it is found that pure O3, O′3 and P′3 phase can only form at a fixed stoichiometry of x = 1.00, 0.83, and 0.67, respectively, while the P2 phase forms in a slightly larger composition range from 0.68 to 0.76. Galvanostatic charging of O3−$Na_{1.00}CoO_2$ shows several flat and sloping regions on the voltage profile, which follows the sequence of O3−O′3−P′3−P3−P′3, with increasing interslab distances. Our results indicate that the electrochemically important P2 structure is likely stabilized by entropy.

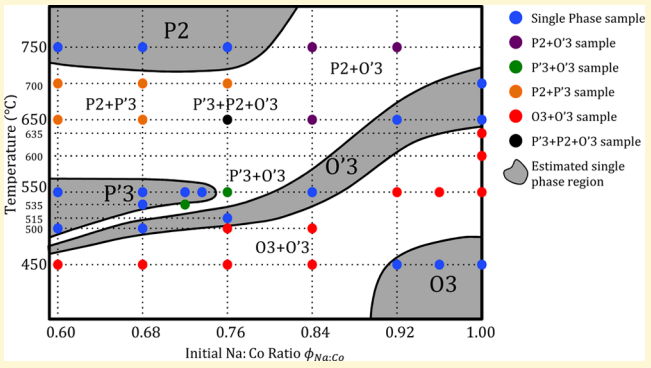

INTRODUCTION

Layered Na_xMO_2 or $Na_xM_{(1)}M_{(2)}...O_2$ (M = transition metal) have been widely studied as cathode materials in sodium ion batteries.[1−5] These compounds can be classified into two major groups, P2 type and O3 type, according to Delmas' notation.[6] The O or P designation refers to the local structure around Na^+ as either an octahedral or prismatic oxygen cage, while the numerical designations refer to the repeat period of the transition metal stacking perpendicular to Na layers. Both structure types have been shown to exhibit good electrochemical performance in Na-ion batteries.[2,3,7,8] The P2 type compounds usually retain the P2 framework, within which various Na vacancy orderings form upon charging or discharging.[4,9−12] At high voltage or low Na content P2−O2 (refs 13, 14.) or P2−OP4 (ref 2), transitions have also been reported. The O3 type compounds usually experience O3−O′3 transitions upon desodiation. In O′3 the symmetry is reduced to monoclinic, probably due to Na vacancy ordering. Transitions to P3/P′3 have been confirmed by in situ or ex situ XRD studies in various systems,[15−20] where the prime in P′3 indicates the structure is a monoclinic distortion of its P3 parent.[6,15]

Several P2 and O3 materials have shown excellent electrochemical behavior,[2,3,8] though first-principles data indicate that the O3 and P2 structures are likely to have different behaviors of the Na ion mobility as a function of state of charge.[13,21,22] Given the different electrochemical behavior of the distinct layered structures we have used Na_xCoO_2 in this study as a prototype to understand the synthesis conditions for the various P2, P′3, O3, and O′3 phases.

The Na_xCoO_2 system had been studied as a cathode material since the 1980s.[15,23] Other fascinating properties of this material include its thermoelectric power[24] and superconductivity in P2−$Na_{0.35}CoO_2{\cdot}1.3H_2O$ (ref 25). The earliest Na_xCoO_2 phase diagram proposed in 1973[26] indicates that four different phases of Na_xCoO_2 can be synthesized by classic solid-state reaction, known as α (also named O3, ref 6), α' (also named O′3 or O1 in the literature, ref 27), β (also named P′3 or P1, ref 27), and γ (also named P2). In addition, Na_xCoO_2 with various x can be obtained by chemical or electrochemical intercalation or deintercalation of sodium ions.[15,27−29] Previous reports on the synthesis of Na_xCoO_2 by solid-state reaction are summarized in Table 1. The P2 phase is usually obtained at higher temperature (650−900 °C) in the composition range $0.55 < x < 0.88$, while the three-layer structures, O3, O′3, and P′3, are obtained for $0.92 < x < 1.00$, $0.75 < x < 0.83$, and $0.60 < x < 0.67$, respectively, and lower T (500 °C−550 °C).

The objective of this paper is to report a phase diagram of Na_xCoO_2, obtained by air quenched samples, in a wide range of temperatures and Na content so that the synthesis conditions of each phase can be identified. For clarity, we define $\phi_{Na:Co}$ as the initial Na:Co ratio between precursors or nominal sodium

Received: June 16, 2014
Revised: August 22, 2014
Published: September 3, 2014

   dx.doi.org/10.1021/cm5021788 | Chem. Mater. 2014, 26, 5288−5296

Table 1. Compositions and Structure Types of Na_xCoO_2 and the Corresponding Solid-State Synthesis Conditions[a]

compound	structure type	synthesis temperature	interslab distance	reference
$Na_{0.88}CoO_2$	P2	900 °C	5.4310 or 5.4040	ref 30
$Na_{0.77}CoO_2$	P2	900 °C	5.4475 or 5.4435	ref 30
$Na_{0.75}CoO_2$	P2	800 °C	-	ref 29
$Na_{0.75}CoO_2$	P2	800 °C	5.4072 or 5.4378	ref 28
$Na_{0.74}CoO_2$	P2	850 °C	-	ref 4
$Na_{0.72}CoO_2$	P2	>650 °C	5.4500	ref 26
$Na_{067}CoO_2$	P2	750 °C	-	ref 23
$Na_{0.66}CoO_2$	P2	900 °C	5.4585	ref 30
$Na_{0.55}CoO_2$	P2	900 °C	5.4735	ref 30
$Na_{1.00}CoO_2$	O3	500 °C	5.1900	ref 26
$Na_{1.00}CoO_2$	O3 (single crystal)	1050−850 °C	5.2030	ref 31
$Na_{0.92}CoO_2$	O3	550 °C	5.1999	ref 27
$Na_{0.83}CoO_2$	O′3	550 °C	-	ref 23
$Na_{0.75}CoO_2$	O′3	550 °C	5.3670	ref 27
$Na_{0.75}CoO_2$	O′3	500 °C	5.3766	ref 26
$Na_{0.67}CoO_2$	P′3	550 °C	-	ref 23
$Na_{0.67}CoO_2$	P′3	530 °C	5.4992	ref 32
$Na_{0.62}CoO_2$	P′3	550 °C	5.4923	ref 33
$Na_{0.62}CoO_2$	P′3	550 °C	5.4922	ref 30
$Na_{0.60}CoO_2$	P′3	550 °C	5.4871	ref 27
$Na_{0.60}CoO_2$	P′3	500 °C	5.5100	ref 26

[a]References 23, 26, 27, and 33 determined x according to initial precursor ratio. References 4, 28, 29, and 32 determined x using ICP (inductively coupled plasma) measurements. Reference 30 determined x according to its dependence of the c parameter either from DFT calculations in reference 34 or single crystal experimental data in reference 35. If there are two values of the interslab distance for one compound, it indicates two phases were observed in the experiment.

content, while x in Na_xCoO_2 stands for the actual sodium composition in a layered phase. The value of "x" was determined by comparing the interslab distance from the ex situ XRD on the synthesized powder samples with the interslab distance measured as a function of Na content upon electrochemical desodiation, obtained from an in situ XRD measurement. In contrast to previous literature, our results show that in solid-state synthesis most phases form at a fixed sodium stoichiometry and that any deviation of $\phi_{Na:Co}$ from that stoichiometry is accommodated by impurity phases. We find that the pure O3 phase, previously reported to exist in the range of $0.90 < x < 1.00$, can only exist as $Na_{1.00}CoO_2$. The O′3 phase with a monoclinically distorted structure only exists as $Na_{0.83}CoO_2$ by solid-state reaction in the $\phi_{Na:Co}$ range from 0.68 to 1.00. Similarly, the P′3 phase forms at a fixed stoichiometry around $Na_{0.67}CoO_2$ between 500 and 550 °C. Pure P2 phase, however, forms with a relatively large range of $0.68 < x < 0.76$ above 750 °C and is likely to be the only of the four phases that forms with a range of possible Na compositions. We also find that the P3 phase which was not observed in direct synthesis can be obtained by electrochemical deintercalation at room temperature near $x = 0.56$ ($\approx 5/9$).

EXPERIMENT

Samples of Na_xCoO_2 in the range $0.60 < \phi_{Na:Co} < 1.05$ were synthesized by solid state reaction at temperatures ranging from 450 to 750 °C. Powders of Na_2O_2 (Alfa, 95%) and Co_3O_4 (Alfa, 99.7%) were mixed in appropriate amounts and thoroughly ground by high-energy ball milling before pressing into the pellets. Samples were treated carefully to minimize the air contact before they were placed in a box furnace. The temperature was increased at 5 °C/min to the target value and held constant for 16 h in air. The samples were then quenched to room temperature by placing them on a Cu foil for 30 s to 1 min and quickly transferred to an Ar-filled glovebox. Thirty-seven samples in total were synthesized using this method. An additional four O3 samples were synthesized at 450 °C in a tube furnace with flowing O_2.

All samples were analyzed by X-ray powder diffraction on a Rigaku Rotaflex or PANalytical X' Pert pro diffractometer equipped with Cu Kα radiation. Data were collected in the 2θ range of 10°−85° at a scan rate of 0.021° s^{-1} or slower. All the XRD samples were sealed using Kapton film to avoid air contact or moisture contamination. The structural information and lattice parameters were determined using Rietveld refinement, as described in detail later. Sodium contents of Na_xCoO_2 phases in all samples were determined by a comparison with in situ XRD results, as described in detail later.

Electrochemical studies and the in situ XRD measurements were carried out on Na/1 M $NaPF_6$ in EC:DEC/O3−$Na_{1.00}CoO_2$ batteries, with a homemade design that enables XRD signals to be collected through a Be window in the cell. The cathode film consists of 80 wt % of active material, 15 wt % of carbon black, and 5 wt % of PTFE as a binder. A glass fiber filter was used as separator. The airtight cells were carefully assembled inside an Ar-filled glovebox to avoid any air or moisture contact. The battery was charged from 2.5 to 3.4 V (corresponding to $1.00 > x > 0.52$) at a rate of C/50 (4.7 mA g^{-1}) at room temperature. The in situ XRD spectra were taken simultaneously on a Bruker D8 X-ray diffractometer equipped with a Mo source ($\lambda_{K\alpha 1}$ = 0.7093 Å). Each scan was carried out at a scanning speed of 0.0065° s^{-1} or 1 h per spectrum in the 2θ range from 6.5° to 30°, corresponding to a 2% Na composition resolution.

RESULTS

Of the 41 samples synthesized in the range of 450 °C < T < 750 °C, $0.60 < \phi_{Na:Co} < 1.05$, 19 contained a single layered phase in XRD while in the other 22 samples more than one type of layered compounds could be identified in the XRD measurements. We refer to the first category as "single phase" samples, though in some cases Co_3O_4 was also present. All four known phases (O3, O′3, P′3, P2) of Na_xCoO_2 were found in this range of synthesis conditions. The results are shown in the experimental synthesis phase diagram (Figure 1). Note that the compositions on the x-axis are the nominal sample composition and not the Na content of the phases formed. The O3 phase clearly forms at lower temperature and with higher $\phi_{Na:Co}$. In agreement with previous literature, P2 appears at higher temperature and for lower $\phi_{Na:Co}$. The P′3 phase can be obtained in a narrow temperature window around 550 °C when sodium is highly deficient, which is consistent with earlier reports listed in Table 1. The O′3 phase, however, can be synthesized over a large range of Na:Co ratios from $\phi_{Na:Co}$= 0.68 (or even lower) to $\phi_{Na:Co}$= 1.00, forming a narrow diagonal band on the synthesis phase diagram. Regions in which two phases could be identified lie between any two single-phase regions. In most of the samples a certain amount of Co_3O_4 impurity could be detected as well.

A. Structural Characterization. For single-phase samples representative of each phase the structural parameters were extracted from the XRD pattern using the Rietveld refinement method (Table 2). The O3 phase $Na_{1.00}CoO_2$ ($\phi_{Na:Co}$ = 1.05, T = 450 °C) has an XRD pattern that can be indexed within the trigonal space group $R\bar{3}m$ (No. 166), while the O′3 sample $Na_{0.83}CoO_2$ ($\phi_{Na:Co}$ = 1.00, T = 650 °C) and the P′3 sample $Na_{0.67}CoO_2$ ($\phi_{Na:Co}$ = 0.68, T = 535 °C) are indexed based on

dx.doi.org/10.1021/cm5021788 | Chem. Mater. 2014, 26, 5288−5296

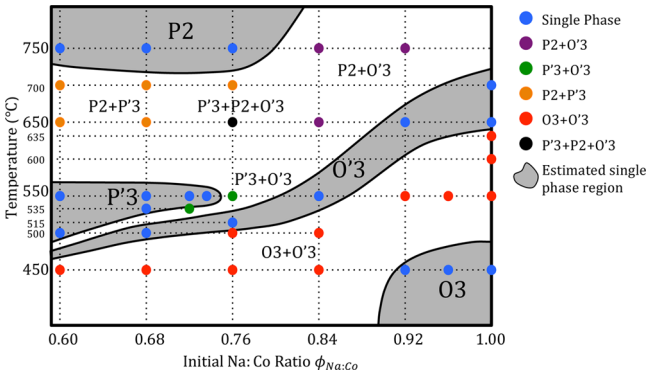

Figure 1. Synthesis phase diagram of Na_xCoO_2 as a function of the precursor Na:Co ratio $\phi_{Na:Co}$ (X axis) and the sintering temperature (Y axis). Since the Na content x in the layered phase Na_xCoO_2 can deviate significantly from the synthesis Na:Co ratio, $\phi_{Na:Co}$ is used in this diagram instead of x. Samples were designated as "single phase" when no other layered structure could be observed in the XRD pattern; however, some of these samples may contain a small amount of Co_3O_4 impurity. Most samples that fall into the two-phase domains contain Co_3O_4.

monoclinic cells in the space group $C2/m$ (No. 12). Both of the P2 phase samples $Na_{0.68}CoO_2$ ($\phi_{Na:Co}$ = 0.68, T = 750 °C) and $Na_{0.76}CoO_2$ ($\phi_{Na:Co}$ = 0.76, T = 750 °C) can be well indexed with a hexagonal cell in the space group $P6_3/mmc$ (No. 194). The XRD patterns and refinements for all four phases are shown in Figure 2.

B. Electrochemical Deintercalation of Na in a Three Layer Series. To obtain the actual Na content x in each layered phase we compare d_{00l}, the interslab distance, obtained from the ex situ XRD with the relation between d_{00l} and x as obtained by in situ XRD in electrochemical charging experiments. Figure 3 shows the voltage, Na content, and diffraction near the O3−003 peak position as the in situ cell is charged. As a consequence of the preferred orientation of the active material in the cathode film, all c-axis related ($00l$) peaks are enhanced while the a or b axis related peaks are suppressed. One can clearly identify O3, O′3, and P′3 single-phase regions, as well as the two-phase regions between them.

By combining the in situ XRD patterns and the voltage profile in Figure 3, we conclude that the short initial sloping region at x = 1.00 and the second sloping region between 0.81 and 0.88 in the voltage curve correspond to the O3 and O′3 single phase domains, respectively. Similarly, the steep step at x = 0.67 marks the start of the P′3 region. The plateaus between these steps characterize the two-phase domains of O3 + O′3 and O′3 + P′3. The nominally P′3 region clearly has a lot of structure to it, and the complex changes of diffraction intensity near $2\theta \approx 26°$(Mo Kα_1 and Kα_2), as well as the small changes in the structure of the voltage profile, indicate that potentially more distinct phases occur in this region. The two small plateaus and step between them near x = 0.56 and the XRD profiles around 2θ = 26° reveal a P′3−P3−P′3 phase transition in a very narrow composition range. Upon charging, the P′3-201 peak and the P′3-$\bar{1}$12 peak join at x = 0.56 and form the P3-015 peak, which splits again into (201) and ($\bar{1}$12) upon further charging, as labeled in the inset of Figure 3. The additional unlabeled peaks nearby are due to Mo Kα_2 radiation. In order to more clearly analyze the P3−$Na_{0.56}CoO_2$ phase, an ex situ XRD was taken on a cathode film electrochemically charged in a Swagelok cell to $Na_{0.56}CoO_2$ (Figure 4) and compared with that of P′3 (Figure 4 inset a) from the solid state synthesis. The monoclinic splitting of the P3 104, 015, 107, and 018 reflections can be clearly observed in P′3 in Figure 4 inset. A Rietveld refinement has also been carried out in space group $R3m$ (No. 160) for the P3 phase and the results are included in Table 2.

In Figure 3 the 003 peaks of the O3 phase have a fixed position, corresponding to a constant interslab distance d_{003} = 5.200 Å, in either the single O3 phase region or in the two-phase region with O′3. In contrast, the 001 peak of the O′3 phase maintains a fixed position in the two-phase regions with O3 and P′3, but an obvious shift of the 001 peak toward low angle (corresponding to an increase in d_{001} interslab distance) is observed in the single-phase domain upon charging. The behavior of the 003 peaks of the P′3 phase is similar to those of O′3, remaining fixed in the two-phase region with O′3 but shifting toward low angle (corresponding to an increase in d_{003} interslab distance) in the single-phase region during charging. This result is consistent with previous reports.[3,15]

C. Delineation of the Single-Phase Domains. *O3.* Four samples with single phase O3 were obtained at 450 °C ($\phi_{Na:Co}$ = 0.92, 0.96, 1.00, 1.05). Their refined parameters as a function

Table 2. Cell Parameters and Synthesis Conditions of Representative Samples for Each Phase of Na_xCoO_2

compound	space group	cell constants (Å)	volume (Å^3)	volume/f.u. (Å^3)	structure type	synthesis conditions	
$Na_{1.00}CoO_2$	$R\bar{3}m$ (No. 166)	a = 2.8883 c = 15.6019	112.718	37.573	O3	$\phi_{Na:Co}$ = 1.05	T = 450 °C
$Na_{0.83}CoO_2$	$C2/m$ (No. 12)	a = 4.8912 b = 2.8681 c = 5.7937 β = 111.84°	75.443	37.722	O′3	$\phi_{Na:Co}$ = 1.00	T = 650 °C
$Na_{0.67}CoO_2$	$C2/m$ (No. 12)	a = 4.9126 b = 2.8270 c = 5.7087 β = 106.06°	76.188	38.094	P′3	$\phi_{Na:Co}$ = 0.68	T = 535 °C
$Na_{0.68}CoO_2$	$P6_3/mmc$ (No. 194)	a = 2.8320 c = 10.8971	75.690	37.845	P2	$\phi_{Na:Co}$ = 0.68	T = 750 °C
$Na_{0.76}CoO_2$	$P6_3/mmc$ (No. 194)	a = 2.8381 c = 10.8265	75.522	37.761	P2	$\phi_{Na:Co}$ = 0.76	T = 750 °C
$Na_{0.56}CoO_2$	$R3m$ (No. 160)	a = 2.8192 c = 16.5880	114.176	38.059	P3	electrochemical deintercalation of Na from O3−$Na_{1.00}CoO_2$	

dx.doi.org/10.1021/cm5021788 | *Chem. Mater.* 2014, 26, 5288−5296

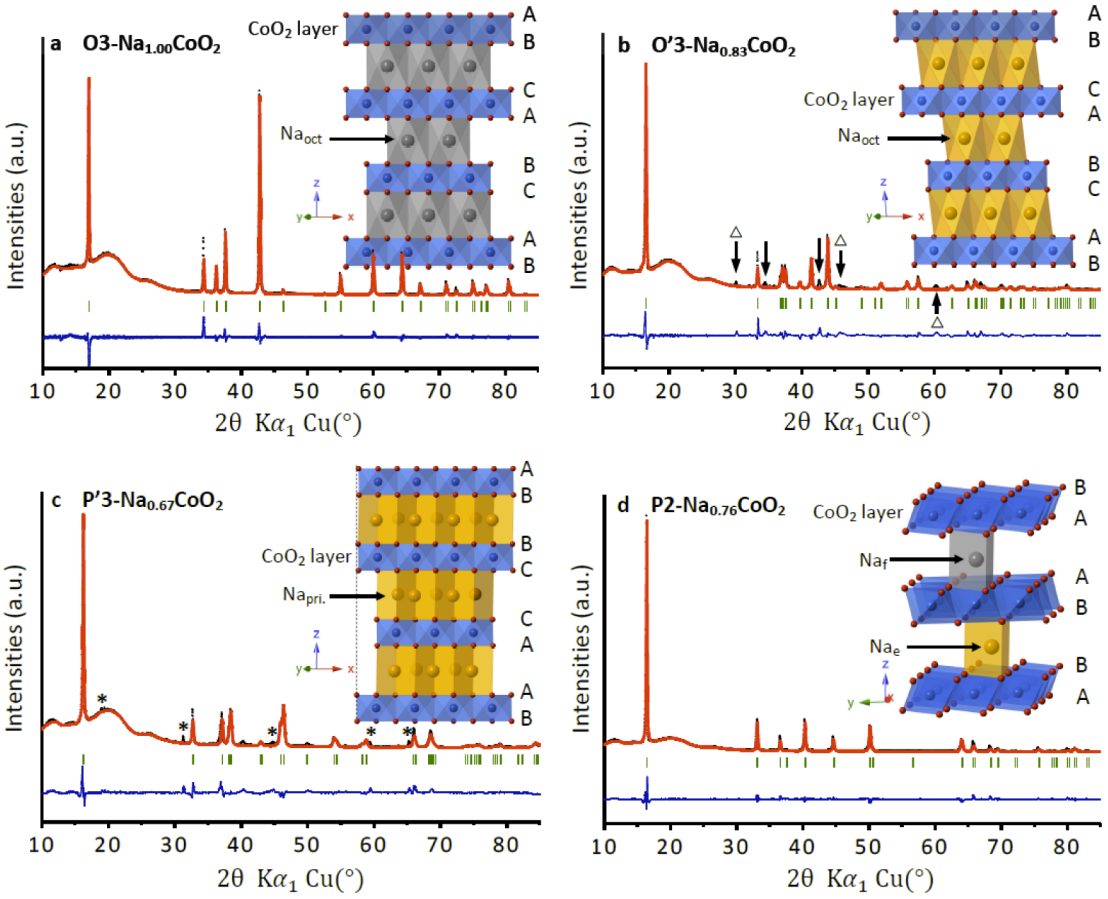

Figure 2. Structural characterization of four different phases of Na_xCoO_2. Observed (black dots) and calculated (red lines) XRD patterns for (a) O3–$Na_{1.00}CoO_2$ (R_{wp} = 14.3%) with $\phi_{Na:Co}$ = 1.05 and T = 450 °C, (b) O′3–$Na_{0.83}CoO_2$ (R_{wp} = 19.8%) with $\phi_{Na:Co}$ = 1.00 and T = 650 °C, (c) P′3–$Na_{0.67}CoO_2$ (R_{wp} = 19.0%) with $\phi_{Na:Co}$ = 0.68 and T = 535 °C, (d) P2–$Na_{0.76}CoO_2$ (R_{wp} = 15.2%) with $\phi_{Na:Co}$ = 0.76 and T = 750 °C. The broad peaks between 10° and 30° are due to the Kapton film used to seal the samples. The residual discrepancy (blue lines) and peak positions (green bars) are given beneath each pattern. Peaks marked by arrows in (b) are suspected to be due to Na ion ordering in the O′3 structure while those with additional triangles are mentioned before (ref 26), and peaks marked with * in (c) are Co_3O_4 impurities. Symbols A, B, and C in the schematics (insets) represent layers of oxygen with different stacking. In the O3 and O′3 structures, all Na ions reside in edge sharing octahedral sites, while in the P′3 structure, Na ions have prismatic coordination with one side edge sharing and another face sharing with a Co octahedron.

of $\phi_{Na:Co}$ are shown in Figure 5a. The O3 structure in all samples has the interslab distance $d_{003} = c_{tri}/3 = 5.200 \pm 0.003$ Å and the a_{tri} lattice constant $a_{tri} = 2.889 \pm 0.001$ Å. In addition, based on a careful examination of the XRD patterns of these four samples, only the sample with $\phi_{Na:Co}$ = 1.05 does not exhibit any impurity peak, while an increasing amount of Co_3O_4 is observed as $\phi_{Na:Co}$ decreases from 1.00 to 0.92, as illustrated in Figure 6a. By comparing the interslab distance of these samples with the in situ measured distances (Figure 7) we conclude that O3–Na_xCoO_2 forms in synthesis only as a stoichiometric phase with $x \approx 1.00$

O′3. Five nominally single-phase samples of O′3 with $\phi_{Na:Co}$ = 0.68, 0.76, 0.84, 0.92, and 1.00 were synthesized at 500 °C, 515 °C, 550 °C, 650 °C, and 650 °C, respectively. Their refined lattice parameters as a function of $\phi_{Na:Co}$ are shown in Figure 5b. Similar to the case of O3, all O′3 samples have the same or very similar interslab distance, $d_{001} = c_{mon} \times \cos(\beta - (\pi/2)) = 5.363 \pm 0.003$ Å, and the same a_{mon} lattice constant, $a_{mon} = 4.896 \pm 0.002$ Å. An examination of the XRD patterns of these five samples shows that the samples with $\phi_{Na:Co} > 0.84$ do not exhibit any Co_3O_4 impurity peak, while an increasing amount of Co_3O_4 is observed as $\phi_{Na:Co}$ decreases from 0.84 to 0.68 in the other three samples (Figure 6b).

P′3. As can be found in Figure 1, six nominally single-phase samples of P′3 with $\phi_{Na:Co}$ = 0.60, 0.68, 0.72, 0.74, 0.60, and 0.68 were synthesized at 550 °C, 550 °C, 550 °C, 550 °C, 500 °C, and 535 °C, respectively. Their refined lattice parameters as a function of $\phi_{Na:Co}$ are shown in Figure 5c. All P′3 samples were also found to have very similar interslab distances, $d_{001} = c_{mon} \times \cos(\beta - (\pi/2)) = 5.480 \pm 0.003$ Å, and almost the same a_{mon} lattice constant, $a_{mon} = 2.824 \pm 0.002$ Å. The XRD patterns of these five samples show the existence of certain amount of Co_3O_4 in all five of P′3 samples. Figure 6c shows the presence of the Co_3O_4 311 peak.

P2. Another three samples with single-phase P2 were obtained at 750 °C ($\phi_{Na:Co}$ = 0.60, 0.68, 0.76). Their refined lattice parameters as a function of $\phi_{Na:Co}$ are shown in Figure 5d. Unlike the other three phases, the results indicate that the samples with $\phi_{Na:Co}$ = 0.60 and $\phi_{Na:Co}$ = 0.68 have the lattice parameters $d_{002} = c_{hex}/2 = 5.451 \pm 0.001$ Å, $a_{hex} = 2.831 \pm 0.001$ Å, while the one with $\phi_{Na:Co}$ = 0.76 has smaller d_{002} but larger a_{hex} ($d_{002} = c_{hex}/2 = 5.403$ Å, $a_{hex} = 2.840$ Å). The XRD patterns confirmed the purity of the samples with $\phi_{Na:Co}$ = 0.68 and 0.76, while the other one, with $\phi_{Na:Co}$ = 0.60, contains a small amount of Co_3O_4 impurity, as shown in Figure 6d.

dx.doi.org/10.1021/cm5021788 | *Chem. Mater.* 2014, 26, 5288–5296

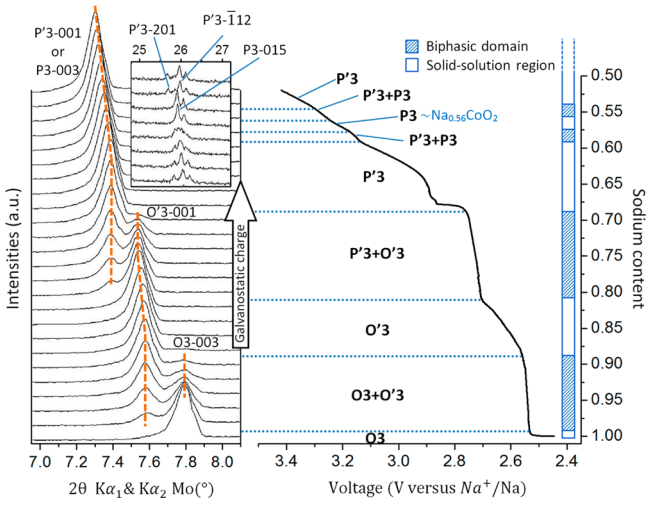

Figure 3. Electrochemistry and in situ XRD of O3−Na_xCoO_2. The galvanostatic electrochemical charge curve (right side) and simultaneous in situ XRD scans (left side) are shown. Note that a Mo-XRD source is used in this experiment. Each XRD scan takes 1 h which corresponds to Δx = 0.02. The resulting in situ XRD experiment shows either solid-solution behavior in the single-phase regions, characterized by a peak shifting, or phase transitions between two phases, characterized by the coexistence of two distinct 00*l* peaks. The combination of 201 and $\bar{1}$12 peaks and the successive splitting of the 015 peak (top left inset) characterize the P′3−P3−P′3 phase transition.

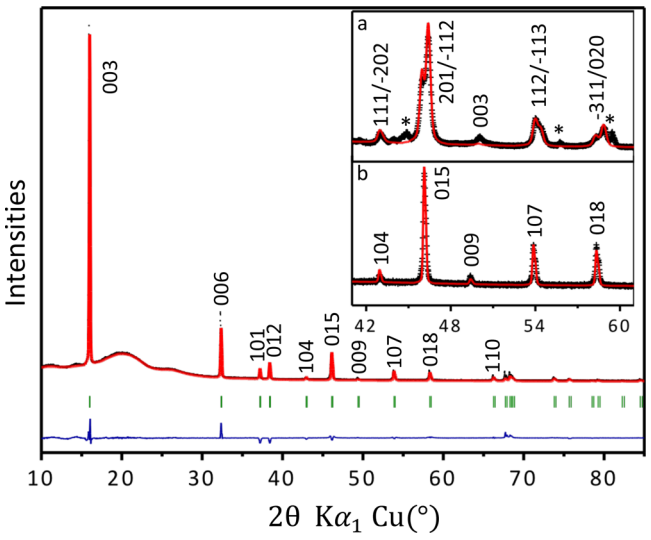

Figure 4. Ex situ XRD characterization of P3−$Na_{0.56}CoO_2$. Observed (black dots) and calculated (red lines) XRD profiles for P3−$Na_{0.56}CoO_2$ are shown. A Rietveld refinement, carried out in space group *R*3*m* (No. 160), gives a = 2.8192 Å, c = 16.5880 Å, R_{wp} = 15.08%. The residual discrepancy (blue lines) and peak positions (green bars) are given beneath the pattern. Observed (crosses) and calculated (red lines) XRD patterns of P′3-$Na_{0.67}CoO_2$ (inset a) and P3−$Na_{0.56}CoO_2$ (inset b) in the range of 41° < 2θ < 61° are compared in detail. Peaks marked by * in inset (a) are due to impurities of Co_3O_4 precursor. Both P3 and P′3 samples are also listed in Table 2.

DISCUSSION

In this paper we established the conditions under which the various phases in Na_xCoO_2 form in solid-state synthesis and establish the actual Na composition of the different layered phases that can form. In the range of 450 °C < T < 750 °C and Na:Co precursor ratio 0.60 < $\phi_{Na:Co}$ < 1.05 we observed the O3, O′3, P′3, and P2 structure. While often the nominal composition of the precursors is taken as the composition of a phase, this can be incorrect due to volatility of species (e.g., Na) or the formation of impurity phases that cannot be detected in XRD. By comparing the ex situ measured lattice parameters of these samples with those measured in situ upon desodiation we were able to establish the actual Na composition of each layered phase. We find that the lattice parameters of O3−Na_xCoO_2 are essentially invariant regardless of the synthesis conditions, indicating that it forms as a stoichiometric phase. By comparing with the in situ data, we believe that this stoichiometry is very close to $Na_{1.00}CoO_2$.

Our findings on O′3 are similar. In contrast to earlier studies on O′3−Na_xCoO_2 (refs 26 and 27), our experiments indicate that the O′3 phase only forms as O′3−$Na_{0.83}CoO_2$ by solid-state reaction, even though the precursor ratio $\phi_{Na:Co}$ can be varied from 0.68 to 1.00. All O′3 samples have $d_{001} \approx$ 5.365 Å as shown in Figure 5b, for which the corresponding sodium composition, x = 0.83, can be easily read from the O′3 d_{001}−x relation in Figure 7. The data point marked as "2" in Figure 7 has the closest interslab distance to the synthesized O′3 samples and corresponds to O′3−$Na_{0.83}CoO_2$. The conclusion that O′3 can only form in the composition $Na_{0.83}CoO_2$ is consistent with the observation of an increasing amount of Co_3O_4 impurity as $\phi_{Na:Co}$ decreases from 0.84 to 0.68, while no additional Co_3O_4 was found in samples with $\phi_{Na:Co}$ > 0.84, indicating that for $\phi_{Na:Co}$ < 0.83 excess Co in the precursor forms Co_3O_4. For $\phi_{Na:Co}$ > 0.83, excess Na should exist. We could not detect any excess Na phases (in any samples), indicating that excess Na may evaporate during sintering or exists in the form of amorphous Na_2O_2 which cannot be detected by XRD. We further confirmed that O′3 obtained by direct synthesis is the same phases as O′3 formed from O3 during room temperature electrochemical desodiation. Figure 8 shows a comparison between the charge curve of an electrode made with an O′3 sample with nominal composition $\phi_{Na:Co}$ = 1.00 and that of an O3 cathode with composition $Na_{1.00}CoO_2$. The two charge curves have been aligned according to the steps and features they share in common at the same voltage. Alignment of the initial potential rise of the O′3 electrode with the similar feature in the charged O3 electrode further confirms that the composition of O′3 is x = 0.83. However, in contrast to the high-temperature synthesis results, it is clear that at room temperature the O′3 phase can exist metastable with other compositions x, from 0.81 to 0.88, corresponding to 5.375 Å > d_{001} > 5.350 Å. This is because the equilibrium is highly constrained at room temperature. Since Co_3O_4 cannot easily form at room temperature, the stability region of the topotactic layered phases becomes substantially larger than in the high-temperature phase equilibrium. Finally, we notice that 0.83 ≈ 5/6, which suggests that O′3−$Na_{5/6}CoO_2$ is a Na-vacancy ordered superstructure of O3 as was first mentioned in 1973[26] and observed by TEM electron diffraction later.[27] The specific ordering in this structure has not yet been identified.

Similar to O3 and O′3 containing samples, we find that all P′3 phases also have almost identical lattice parameters, as shown in Figure 5c, indicating a very narrow composition range for the P′3 phase. Unlike the other three phases, all P′3 samples contain a small amount of Co_3O_4 impurity (Figure 6c). The interslab distance for P′3 d_{001} = 5.480 Å corresponds to x = 0.67 in the in situ XRD experiment. This composition, marked as "1" in Figure 7, sits very near the boundary between the

dx.doi.org/10.1021/cm5021788 | *Chem. Mater.* 2014, 26, 5288−5296

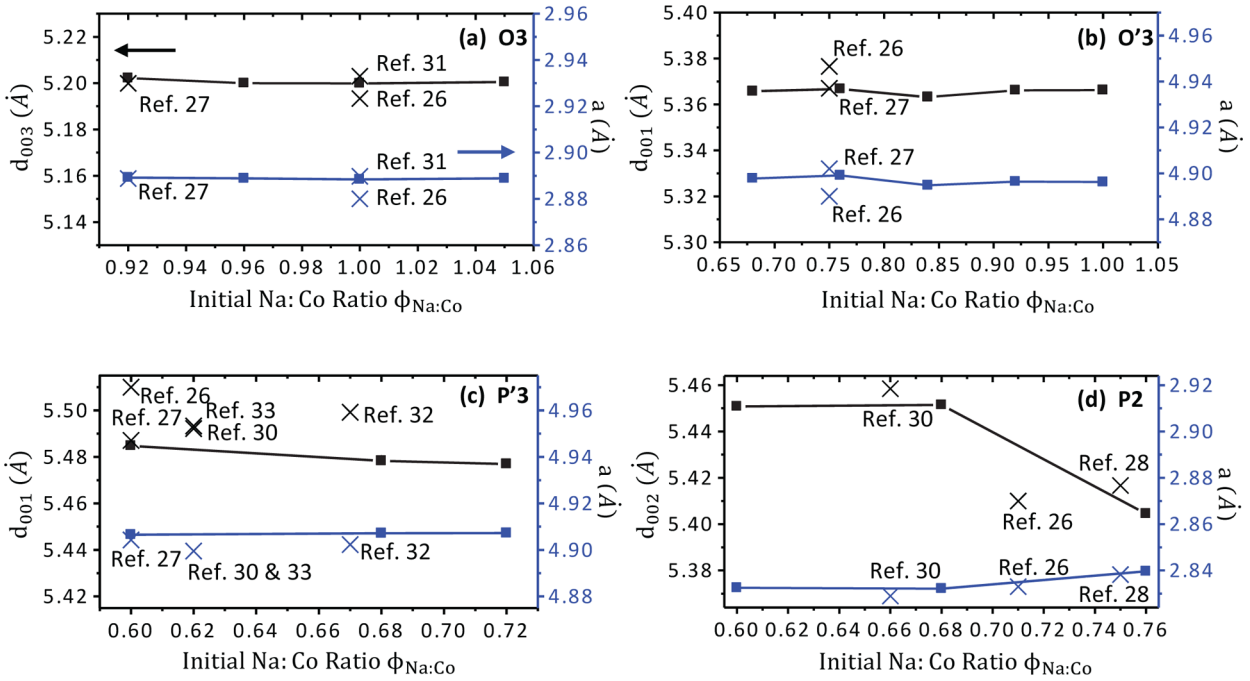

Figure 5. Variations of interslab distance d_{00l} (in black) and horizontal lattice constant a (in blue) as a function of initial Na:Co ratio for O3 (a), O′3 (b), P′3 (c), and P2 (d) samples in nominal single-phase regions. Filled squares indicate data measured in this study, while crosses represent data from literature. Four of the O3 samples, three of the P′3 samples, and three of the P2 samples in (a), (c), and (d) were obtained at 450 °C, 550 °C, and 750 °C, respectively. The five O′3 samples in (b) were synthesized at 500 °C, 515 °C, 550 °C, 650 °C and 650 °C with $\phi_{Na:Co}$ increasing with T. The constant nature of d_{00l} and a found in O3, O′3, and P′3 indicates that these samples have almost the same x regardless of different $\phi_{Na:Co}$. Only P2 samples exhibit variable lattice parameters as a function of $\phi_{Na:Co}$. The comparison of our results (filled squares) with previous experimental studies (crosses) shows good agreement on O3, O′3, and P2 phases, while our P′3 samples exhibit slightly smaller d_{00l} in all compositions, which may indicate our P′3 samples have more Na than the nominal values. The result of ref 28 in (d) is a calculated average value based on their data, and ref 31 in (a) is a single crystal O3 sample.

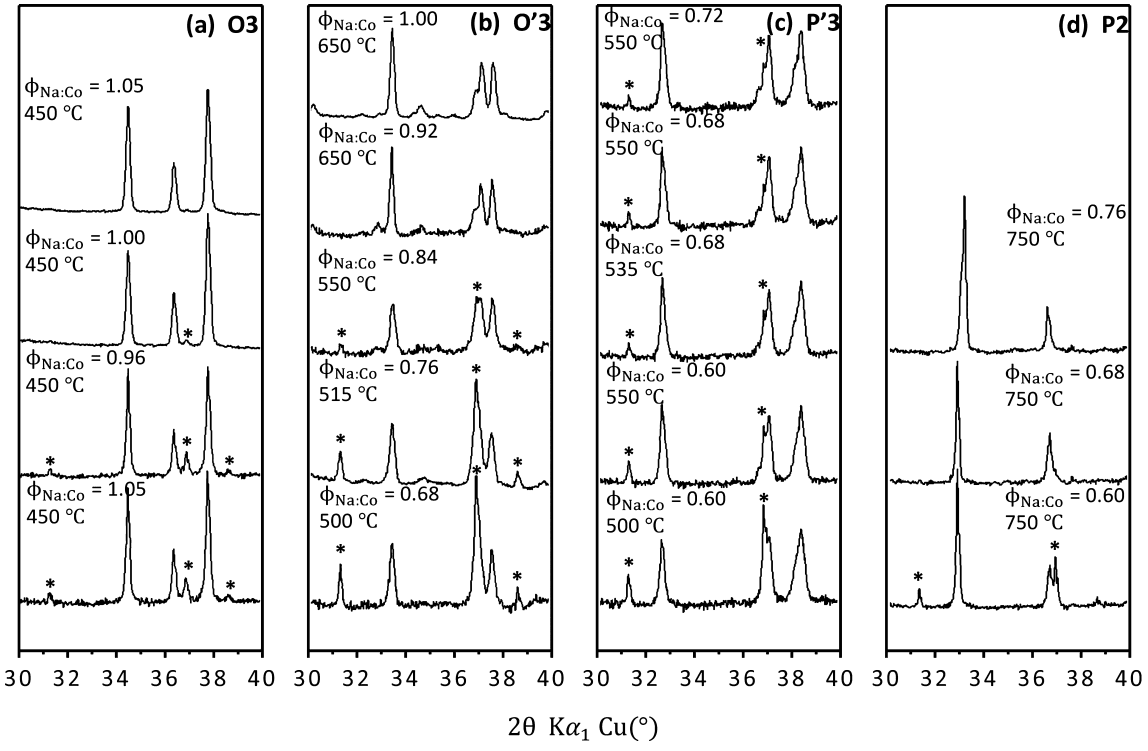

Figure 6. Comparison of the XRD patterns of O3 (a), O′3 (b), P′3 (c), and P2 (d) samples in the nominal single-phase regions from 30° to 40°. Peaks marked by * are Co_3O_4 impurities.

dx.doi.org/10.1021/cm5021788 | *Chem. Mater.* 2014, 26, 5288−5296

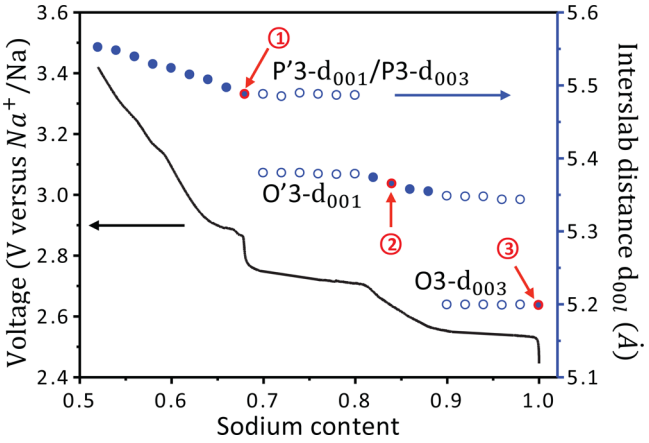

Figure 7. Interslab distance d_{00l} of O3, O′3, and P3/P′3 and voltage as a function of sodium content x as obtained from the in situ electrochemical desodiation. The points in red circles labeled with 1, 2, and 3 give the slab distances that are closest to the interslab distances of the P′3, O′3, and O3 samples synthesized by solid-state reaction.

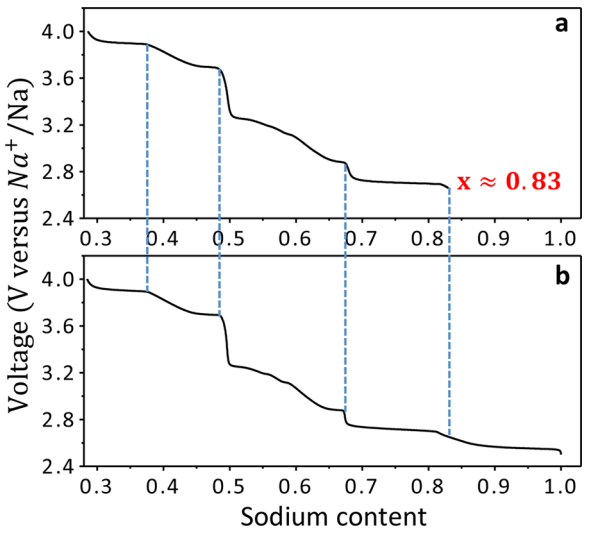

Figure 8. Comparison between the galvanostatic charge curves from (a) O′3–Na_xCoO_2 synthesized at T = 650 °C, $\phi_{Na:Co}$ = 1.00, and (b) O3–$Na_{1.00}CoO_2$ at T = 450 °C, $\phi_{Na:Co}$ = 1.05. Both batteries were charged to 4.0 V at the rate of C/20 at room temperature. The charge curve of O′3 matches that of O3 if the two curves are aligned according to the specific voltage features (blue dashed lines). By shifting the O′3 curve and making it overlap with that of the O3, the initial composition in O′3–Na_xCoO_2 $x \approx 0.83$ could be identified.

single phase P′3 region and the two-phase P′3 + O′3 domain. This indicates P′3 can only form as stoichiometric $Na_{0.67}CoO_2$ when made by solid-state reaction in air.

Among the four layered Na_xCoO_2 phases synthesized by solid-state reaction in this work, P2 phase is the only phase that is found to exist in a relatively large range of Na content of 2/3 < x < 3/4. An obvious d_{002} spacing increase is observed when $\phi_{Na:Co}$ decreases from 0.76 to 0.68, as shown in Figure 5d, which is consistent with an actual Na content decrease in the layered structure in these samples. The nominal Na content of the P2–$Na_{0.68}CoO_2$ and P2–$Na_{0.76}CoO_2$ samples should be very close to the actual Na content in the layered structure, which is not only supported by the purity of their XRD patterns, as shown in Figure 6d, but also by comparing the P2 d_{002}–x relation with that of an in situ XRD experiment on P2 reported previously.[4,34,35] In the synthesis range 0.60 < $\phi_{Na:Co}$ < 0.68, however, P2–$Na_{0.68}CoO_2$ forms and coexists with excess Co in the form of Co_3O_4 identified by the Co_3O_4 311 peak in the XRD pattern of P2 with $\phi_{Na:Co}$ = 0.60 (Figure 6d). The lack of variation in the P2 d_{002} spacing for 0.60 < $\phi_{Na:Co}$ < 0.68 further indicates that the P2 phase obtained in this range has constant Na content, around 0.68 or 2/3. Hence, it seems that the P2 phase can easily exist with Na-excess, but not with Na-deficiency away from its stoichiometry of 2/3.

Finally, an attempt to construct a phase diagram with the actual Na composition in the Na_xCoO_2 phases is shown in Figure 9. The single-phase domains are based on the sodium

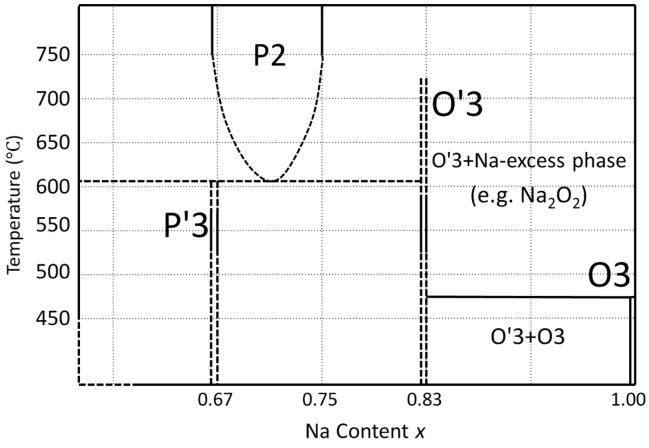

Figure 9. Phase diagram of Na_xCoO_2 as a function of x and the sintering temperature. The single-phase regions of O3, O′3, P′3, and P2 are labeled in the figure while the unlabeled areas stand for multiphase regions. Solid phase boundaries are supported by data, while dashed lines are plausible extrapolations.

content of the layered compounds as determined by the method described above. Each of O3, O′3, and P′3 phases exists at a single composition near x = 1.00, 0.83, and 0.67, respectively, while the P2 phase spans from 0.67 to 0.75 at 750 °C in the phase diagram. The fact that P2 is a high temperature phase with considerable off-stoichiometry suggests that it is entropy stabilized. This may not be surprising since a "P" lattice leads to twice the number of possible Na sites than an "O" lattice. While at low T this is not important as Na only prefers occupation of the prismatic site (Na1 site) that is not face sharing with the Co-octahedron, at high T Na-disorder will lead to some occupancy of the Na2 site. As there are more sites in P2, its ability to generate entropy is higher. This phenomenon is similar to the O2–T2–O6 transition observed in O2–$LiCoO_2$ (ref 36). We expect this entropy stabilization to be generic to all P2 compounds, and, hence, high T will always promote them in synthesis.

It is worth noting that the phase diagram in Figure 9 is constructed from samples synthesized in air and then quenched to room temperature. Such quenched samples are the best representation of the high-temperature state. It is known that the oxygen partial pressure during the high temperature synthesis can also influence the sodium content.[23] We find that a continuous oxygen gas flow usually decreases the Na content and gives an increased interplanar distance compared with the air quenched sample. We also notice that the O′3 phase in ref 26 and P′3 phase in refs 30 and 33 were synthesized under oxygen gas flow, and a comparison of their

dx.doi.org/10.1021/cm5021788 | Chem. Mater. 2014, 26, 5288–5296

lattice parameters and Na compositions agrees well with the relationship determined in this paper.

We now discuss in some detail the transformations that occur upon room temperature electrochemical desodiation and how they are different from the equilibria during synthesis. As reported in the literature[15−20] for various systems, an O3−O′3−P3/P′3 transition in the three-layer structure is typical upon electrochemical deintercalation of Na ions. Our in situ XRD study (Figure 3) clearly unveils the phase evolution of the three-layered type Na_xCoO_2 during sodium deintercalation. Starting with a pure O3 phase, the intensity of the reflection corresponding to the O3 phase 003 plane at $2\theta = 7.795°$ decreases immediately upon charging with an increase in the intensity of the peak at $2\theta = 7.580°$, indicating the transformation of O3 into O′3 in the range of $0.88 < x < 1$. This room temperature behavior is consistent with the lack of off-stoichiometry observed in O3 synthesis. The O3−O′3 transformation is a monoclinic distortion that likely results from Na-vacancy ordering. Upon further Na ion deintercalation, the intensity of the O′3−001 peak decreases accompanied by an increase in the intensity of the P′3−001 peak at $2\theta = 7.382°$, indicating the O′3−P′3 transformation in the range of $0.67 < x < 0.81$. At room temperature, the off-stoichiometry range for O′3 is much larger than at synthesis temperature where any Na-deficiency in O′3 has to compete with Co_3O_4 formation. At room temperature, Co_3O_4 cannot form from O′3 and Na deficiency only has to compete with P′3 formation. As a result, the phase domain of O′3 is considerably larger. On further deintercalation of Na ions in the range $0.54 < x < 0.56$ and $0.57 < x < 0.59$, the successive transitions of P′3−P3 and P3−P′3 can be identified as the combination of the P′3−201 and P′3−$\bar{1}$12 peaks followed by the monoclinic splitting of the P3−015 peak, as shown in Figure 3, top left inset. The reason for this transition is still unknown, but we notice that a previous study has indicated that the P′3−P3 transition in the Na_xCoO_2 system may be attributed to the disordering of Na and vacancies upon heating,[33] indicating that P′3 is likely a Na vacancy ordering superstructure of P3. It is possible that P′3 for $x < 0.56$ and P′3 for $x > 0.57$ are not the same structures, differing in their Na-vacancy ordering.

Our work shows the importance of carefully determining the Na content of each phase. Previous work has tried to correlate the Na composition with the *c* lattice parameter obtained from either DFT simulation or single crystal experimental data.[30] In this work, we used information obtained from in situ XRD to calibrate the Na content of compounds synthesized by solid-state reaction. The in situ XRD measures the interslab distances upon sodium deintercalation at different sodium compositions, which can be compared to the one obtained from XRD refinements of compound synthesized by solid-state reaction to determine its Na composition. In previous work, the Na composition of the synthesized compounds was often estimated based on the initial precursor ratio[23,26,27,33] which may be different from the real Na content in the layered structure due to volatility of the precursor or existence of impurity phase. Even measurements of the Na to transition metal ratio by ICP (inductively coupled plasma)[4,28,29,32] determine at best the composition of the sample, not the composition of the relevant phase.

■ CONCLUSION

In this work, a high-temperature phase diagram of Na_xCoO_2 is constructed from 41 samples of Na_xCoO_2 with $0.60 < \phi_{Na:Co} < 1.05$ synthesized between 450 and 750 °C, revealing four nominally single phase domains and four two-phase regions. All four phases of Na_xCoO_2 reported earlier by solid-state reaction, α (also O3), α' (also O′3 or O1), β (also P′3 or P1), and γ (also P2), were obtained in this work. We find that O3, O′3, and P′3 synthesized by air quenched solid-state reaction only form in fixed stoichiometry as O3−$Na_{1.00}CoO_2$, O′3−$Na_{0.83}CoO_2$, and P′3−$Na_{0.67}CoO_2$, respectively. The P2 phase, on the other hand, can form with a relatively large variation in sodium content, from P2−$Na_{0.68}CoO_2$ to P2−$Na_{0.76}CoO_2$. These phase compositions were obtained in a novel way by combining ex situ diffraction with in situ diffraction during electrochemical desodiation. Our work shows that the room temperature single-phase domains obtained from electrochemical data are considerably larger than the ones that can be achieved in high-temperature solid-state synthesis and that caution should be used when assuming that the precursor ratios actually give the single-phase composition. We expect these conclusions to also hold for other Na_xMO2 systems and believe that our work may serve as a rational design guideline for creating high-energy density Na−metal−cathode materials.

■ AUTHOR INFORMATION

Corresponding Author

*E-mail: gceder@mit.edu

Notes

The authors declare no competing financial interest.

■ ACKNOWLEDGMENTS

This work was supported by the Samsung Advanced Institute of Technology. We also acknowledge Nancy Twu and Alexandra Toumar for helpful discussion.

■ REFERENCES

(1) Li, X.; Ma, X.; Su, D.; Liu, L.; Chisnell, R.; Ong, S. P.; Chen, H.; Toumar, A.; Idrobo, J.-C.; Lei, Y.; et al. *Nat. Mater.* **2014**, *13*, 586−592.

(2) Yabuuchi, N.; Kajiyama, M.; Iwatate, J.; Nishikawa, H.; Hitomi, S.; Okuyama, R.; Usui, R.; Yamada, Y.; Komaba, S. *Nat. Mater.* **2012**, *11*, 1−6.

(3) Yoshida, H.; Yabuuchi, N.; Komaba, S. *Electrochem. Commun.* **2013**, *34*, 60−63.

(4) Berthelot, R.; Carlier, D.; Delmas, C. *Nat. Mater.* **2011**, *10*, 74−80.

(5) Guignard, M.; Didier, C.; Darriet, J.; Bordet, P.; Elkaïm, E.; Delmas, C. *Nat. Mater.* **2012**, *11*, 1−7.

(6) Delmas, C.; Fouassier, C.; Hagenmuller, P. *Physica B+C* **1980**, *99*, 81−85.

(7) Ma, X.; Chen, H.; Ceder, G. *J. Electrochem. Soc.* **2011**, *158*, A1307.

(8) Vassilaras, P.; Toumar, A. J.; Ceder, G. *Electrochem. Commun.* **2014**, *38*, 79−81.

(9) Shu, G.; Chou, F. *Phys. Rev. B* **2008**, *78*, 3−6.

(10) Zandbergen, H.; Foo, M.; Xu, Q.; Kumar, V.; Cava, R. *Phys. Rev. B* **2004**, *70*, 1−8.

(11) Roger, M.; Morris, D. J. P.; Tennant, D. A.; Gutmann, M. J.; Goff, J. P.; Hoffmann, J.-U.; Feyerherm, R.; Dudzik, E.; Prabhakaran, D.; Boothroyd, A. T.; et al. *Nature* **2007**, *445*, 631−4.

(12) Meng, Y. S.; Hinuma, Y.; Ceder, G. *J. Chem. Phys.* **2008**, *128*, 104708.

(13) Lee, D. H.; Xu, J.; Meng, Y. S. *Phys. Chem. Chem. Phys.* **2013**, *15*, 3304−12.

(14) Lu, Z.; Dahn, J. R. *J. Electrochem. Soc.* **2001**, *148*, A1225−A1229.

(15) Delmas, C.; Braconnier, J.; Fouassier, C.; Hagenmuller, P. *Solid State Ionics* **1981**, *3*−*4*, 165−169.

(16) Sathiya, M.; Hemalatha, K.; Ramesha, K.; Tarascon, J.-M.; Prakash, A. S. *Chem. Mater.* **2012**, *24*, 1846−1853.
(17) Saadoune, I.; Maazaz, A.; Menetrier, M.; Delmas, C. *J. Solid State Chem.* **1996**, *122*, 111−117.
(18) Komaba, S.; Yabuuchi, N.; Nakayama, T.; Ogata, A.; Ishikawa, T.; Nakai, I. *Inorg. Chem.* **2012**, *51*, 6211−6220.
(19) Zhou, Y.-N.; et al. *J. Mater. Chem. A* **2013**, *1*, 11130−11134.
(20) Takeda, Y.; et al. *Mater. Res.* **1994**, *29*, 659−666.
(21) Ong, S. P.; et al. *Energy Environ. Sci.* **2011**, *4*, 3680.
(22) Mo, Y.; Ong, S. P.; Ceder, G. *Chem. Mater.* **2014**, DOI: 10.1021/cm501563f.
(23) Shacklette, L. W.; Jow, T. R.; Townsend, L. *J. Electrochem. Soc.* **1988**, *135*, 2669−2674.
(24) Terasaki, I.; Sasago, Y.; Uchinokura, K. *Phys. Rev. B* **1997**, *56*, 685−687.
(25) Takada, K.; Sakurai, H.; Takayama-Muromachi, E.; Izumi, F.; Dilanian, R. A.; Sasaki, T. *Nature* **2003**, *422*, 53−55.
(26) Fouassier, C.; Matejka, G.; Reau, J.; Hagenmuller, P. *J. Solid State Chem.* **1973**, *6*, 532−537.
(27) Viciu, L.; Bos, J. W. G.; Zandbergen, H. W.; Huang, Q.; Foo, M. L.; Ishiwata, S.; Ramirez, A. P.; Lee, M.; Ong, N. P.; Cava, R. J. *Phys. Rev. B* **2006**, *73*, 174104.
(28) Huang, Q.; Foo, M. L.; Pascal, R. A., Jr.; Lynn, J. W.; Toby, B. H.; He, T.; Zandbergen, H. W.; Cava, R. J. *Phys. Rev. B* **2004**, *70*, 184110.
(29) Huang, Q.; Foo, M. L.; Lynn, J. W.; Zandbergen, H. W.; Lawes, G.; Wang, Y.; Toby, B. H.; Ramirez, A. P.; Ong, N. P.; Cava, R. J. *J. Phys.: Condens. Matter* **2004**, *16*, 5803−5814.
(30) Carlier, D.; Blangero, M.; Ménétrier, M.; Pollet, M.; Doumerc, J.-P.; Delmas, C. *Inorg. Chem.* **2009**, *48*, 7018−7025.
(31) Takahashi, Y.; Gotoh, Y.; Akimoto, J. *J. Solid State Chem.* **2003**, *172*, 22−26.
(32) Ono, Y.; Ishikawa, R.; Miyazaki, Y.; Ishii, Y.; Morii, Y.; Kajitani, T. *J. Solid State Chem.* **2002**, *166*, 177−181.
(33) Blangero, M.; Carlier, D.; Pollet, M.; Darriet, J.; Delmas, C.; Doumerc, J.-P. *Phys. Rev. B* **2008**, *77*, 184116.
(34) Hinuma, Y.; Meng, Y.; Ceder, G. *Phys. Rev. B* **2008**, *77*, 224111.
(35) Shu, G.; Prodi, A.; Chu, S. Y.; Lee, Y. S.; Sheu, H. S.; Chou, F. C. *Phys. Rev. B* **2007**, *76*, 184115.
(36) Carlier, D.; Delmas, C.; Ceder, G. *Chem. Mater.* **2003**, *15*, 2651−2660.